JPE 10-3-3

An Isolated Soft-Switching Bidirectional Buck-Boost Inverter for Fuel Cell Applications

Lianghua Zhang†, Xu Yang*, Wenjie Chen*, and Xiaofeng Yao*

†* School of Electrical Engineering, Xi'an Jiaotong University, Shaanxi, China

Abstract

This paper presents a new isolated soft-switching bidirectional buck-boost inverter for fuel cell applications. The buck-boost inverter combines an isolated DC-DC converter with a conventional inverter to implement buck-boost DC-DC and DC-AC conversion. The main switches achieve zero voltage switching and zero current switching by using a novel synchronous switching SVPWM and the volume of the transformer in the forward and fly-back mode is also minimized. This inverter is suitable for wide input voltage applications due to its high efficiency under all conditions. An active clamping circuit reduces the switch's spike voltage and regenerates the energy stored in the leakage inductance of the transformer; therefore, the overall efficiency is improved. This paper presents the operating principle, a theoretical analysis and design guidelines. Simulation and experimental results have validated the characteristics of the buck-boost inverter.

Key Words: Active voltage clamping, Buck-boost inverter, Fuel cell power-conditioning system, Synchronous switching SVPWM

I. INTRODUCTION

With the increase in demand for clean energy applications, fuel cells, as one of the more promising sources, draw more and more attention in the power electronics community. The reason for this attention is that fuel cells convert chemical energy into electrical energy with no pollution, high efficiency and low noise [1]. Unfortunately, some inherent drawbacks exist in fuel cell applications [1]–[3]. These include an output voltage that varies widely with age and output current, and a low-frequency current ripple that reduce conversion efficiency. In addition, fuel cells spend take some minutes to cold start and they respond slowly to step loads. In order to maximize fuel cell efficiency, the operating point of a fuel-cell stack should approach the maximum power-delivery point. For re-generative fuel-cell applications, bidirectional power capability is necessary to generate hydrogen and oxygen. Thus, fuel cell Power-Conditioning Systems (PCS) should exhibit the following characteristics [1]–[3].

- PCSs should boost and regulate the low DC voltage from a fuel cell to a high DC voltage with a small current ripple and they should convert DC to AC for electric utility interfaces, automotive applications, and stationary loads.
- PCSs should allow for wide voltage regulation and be suitable for high-power systems.
- To satisfy domestic and international safety standards for electronic equipment, an isolated transformer is required for a higher voltage or higher power PCS.
- Secondary energy sources and energy storage are necessary for fast response during transients and start-up.
- PCSs should operate efficiently under all conditions and add little to the system cost.

Because conventional inverters cannot satisfy all of these requirements, it is urgent that a new circuit topology for fuel cell PCSs be devloped. The presented circuit topologies from the power electronics scientific community are divided into two groups, which are: 1) multi-stage topologies [3]–[15] and 2) single stage topologies [16]–[23].

The multi-stage topologies usually consist of a front dc-dc converter and a dc-ac inverter. The front dc-dc converter for a PCS boosts the wide-drop voltage of a fuel cell to a higher level for the dc-ac inverter. The proposed front-end dc-dc converters are classified as boost converters [3]- [5], push-pull converters [6], [7], half bridge converters [8], full-bridge converters [9]–[16], wide input and high step-up dc-dc converters [17], [18] or a LLC resonant converter [19]. In addition, conventional hard switching inverters [11], [12], [14], soft-switching inverters [6], [15] and high frequency link inverters [3], [4] have been presented as dc-ac inverters for PCSs. However, in the multi-stage topologies, it is not easy to achieve low cost and high efficiency due to the large number of power switches and the multiple electric energy processing.

In single stage topologies, voltage source [20], [21] and current source [22], [23] buck-boost inverters have been researched as fuel cell PCSs. However, these converters have the limitations of a small voltage gain and no isolation. A Z-source inverter [24] has been presented for fuel cell applications, but three-phase inverters operate with hard switching and do not

Manuscript received Dec. 9, 2009; revised Apr. 3, 2010
† Corresponding Author: lilienthal_zhang@163.com
Tel: +086-29-82665223, Fax: +086-29-82665223, Xi'an Jiaotong Univ.
* School of Electrical engineering, Xi'an Jiaotong University, China

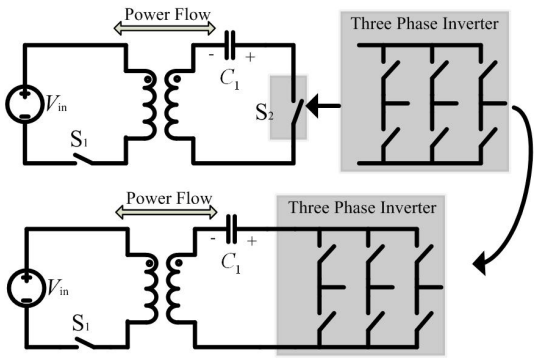

(a) Derivation of the topology

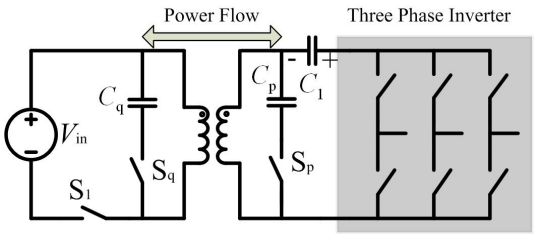

(b) Buck-Boost Inverter with active clamping circuit

Fig. 1. Buck-Boost Inverter.

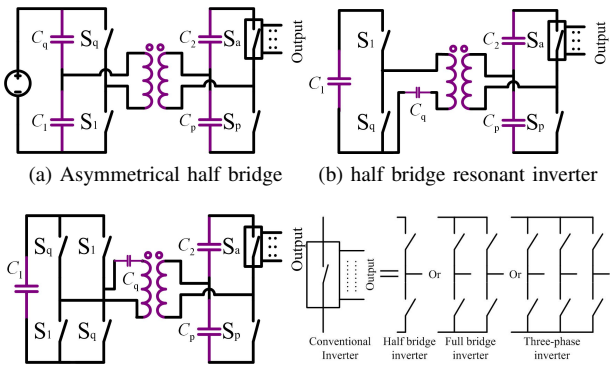

(a) Asymmetrical half bridge (b) half bridge resonant inverter

(c) full bridge resonant inverter (d) conventional inverter

Fig. 2. The derivate topological family.
(: Switching devices - IGBT, MOSFET, DIODE, IGCT etc or the combination of the switches.)

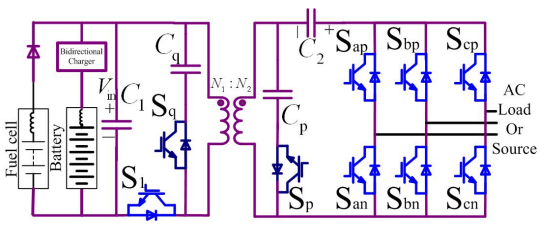

Fig. 3. The proposed three-phase buck-boost inverter for fuel cell PCS.

implement electrical isolation. Although many papers [25], [26] have introduced high-frequency link inverters to minimize the transformer volume or the dc link capacitors, complexity and component cost detract from these topologies.

This paper presents a novel isolated soft-switching bidirectional buck-boost inverter for fuel cell applications. A conventional inverter displaces one or more of the switches of an isolated DC-DC converter to boost the input voltage to a higher level and to invert it to AC voltage with soft switching. By means of a novel synchronous switching SVPWM, the magnetizing inductance current freewheels through the anti-parallel diode of the main switches. Therefore, the switches of a conventional inverter achieve Zero Voltage Switching (ZVS) and Zero Current Switching (ZCS). The active clamping circuit reduces the spike voltage of the switches and recovers the leakage inductance energy. The experimental results from a 1.5 kW prototype confirm the theoretical analysis. The proposed inverter is a good alternative to wide input voltage applications.

II. The Buck-Boost Inverter

Fig.1 shows an isolated bidirectional buck-boost inverter (BBI). The proposed topology is derived by using a conventional three-phase voltage source inverter to replace one switch of a bidirectional fly-back converter. In this topology, the voltage source inverter works as a turned-off switch in the inverting state, and it works as a turned-on switch in the shooting-through state. A conventional half-bridge inverter, a full-bridge inverter or some other multi-phase inverter operates as voltage source inverters. The transformer of a BBI is very different from that of a fly-back converter because it operates in both the forward and fly-back mode. To reduce the switch's spike voltage caused by the leakage inductance of the transformer, fig.1 (b) illustrates the active clamping circuits, where S_p and the capacitor C_3 clamp the switch's voltage in a three-phase inverter, and S_q and the capacitor C_4 clamp the voltage of S_1.

Based on this concept, we derived the topological family of a buck-boost inverter using another isolated DC-DC converter. The isolated DC/DC converter employs a half bridge topology or a full bridge topology with a high frequency transformer, as shown in Fig. 2. The voltage source inverters illustrated in Fig.2 (d) replace one or more of the switches of the isolated DC/DC converter. Fig. 2 (a) shows a derivative topology using an asymmetrical half bridge converter, where the input voltage changes within a narrow range. When a resonant converter based on a half bridge or a full bridge is combined with a conventional voltage source inverter, the other topologies are derived as shown in Fig.2 (b)-(c). Besides the above configurations, any other capacitor can connect with the DC voltage source supplied from a battery, fuel cell or rectifier, while the inverter's output connects with a utility grid, a generator or some other load.

This paper presents a three-phase buck-boost inverter (BBI) for a fuel cell PCS to analyze the operation of the topological family of buck-boost inverters. A detailed configuration of the derived topology is shown in Fig. 3. The parallel battery acts as a secondary energy source for fast responses during transients and start-up. The bidirectional charger is used to charge or discharge the battery efficiently. When the AC load operates in regeneration, the battery is charged through the bidirectional BBI. When the fuel cell's output voltage drops with the load current, the duty cycle of S_1 is controlled to regulate the dc link voltage of the three-phase inverter and maintain the AC output.

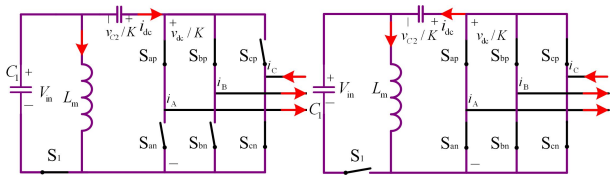

(a) Inverting state (b) Shooting-through zero state

Fig. 4. Two kinds of switching state in buck-boost mode.

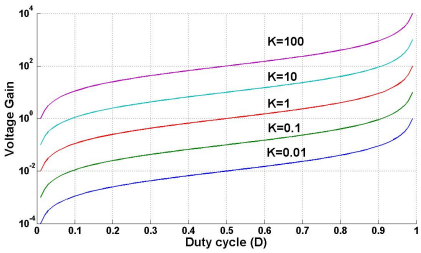

Fig. 5. Voltage gain as a function of duty cycle D.

III. Operating Principles and Circuit Analysis

To simplify the circuit analysis, the equivalent circuit of a BBI operating in buck-boost mode neglects the active clamping circuit, as shown in Fig. 4. The electrical parameters are transferred to the primary side, where the turn's ratio *K* is equal to N_2/N_1 and the inductance L_m is the transformer's magnetizing inductance. In this analysis, it is assumed that the BBI operates at the steady state in one switching cycle. In addition, this analysis neglects the slight impact from the leakage inductance of the transformer.

Based on these assumptions, the circuit operation in one switching cycle can be divided into two kinds of switching states. One is the inverting state and the other is the shooting-through zero state. *D* is defined as the switching-on duty cycle of S_1, v_{Lm} is the magnetizing inductance voltage, v_{C1} and v_{C2} are the capacitors' voltages. In a three-phase inverter, v_{dc} is the dc link voltage and i_{dc} is the dc link current. The arrowheads indicate the current direction.

A. Inverting state

S_1 is turned ON while the inverter is OFF (S_1=1, S_{xp} & S_{xn}=0, e.g. S_{abcp}=110, S_{abcn}=001), as shown in Fig. 4 (a). The voltage sources v_{c1} and v_{c2} act as the dc link voltage together for the three-phase inverter. It is obvious that the transformer operates in both the forward and fly-back modes.

From the equivalent circuit, we can derive that:

$$L_m \frac{di_{L_m}}{dt} = v_{C_1} \tag{1}$$

$$v_{dc} = K v_{C_1} + v_{C_2}. \tag{2}$$

B. Shooting-through zero state

The inverter is turned ON while S_1 is OFF (S_1=0, S_{abcp}=111, S_{abcn}=111), as shown in Fig. 4 (b). The current of the inductance charges the capacitor C_2.

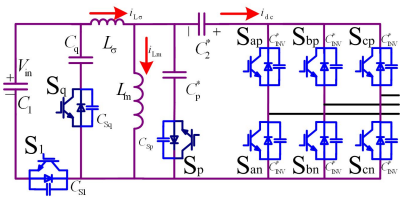

Fig. 6. The BBI's equivalent circuit.

According to the circuit principle, the formulas are derived as:

$$L_m \frac{di_{L_m}}{dt} = -\frac{v_{c_2}}{K} \tag{3}$$

$$v_{dc} = 0. \tag{4}$$

The magnetizing inductance average voltage during one switching period T should be zero at the steady state. From equations (1) and (3), the voltage gain G is described by (5). Fig. 5 shows the voltage gain curve under different turn's ratios, where G is continuously regulated by the duty cycle *D*.

$$G = \frac{v_{C_2}}{v_{in}} = \frac{v_{C_2}}{v_{C_1}} = \frac{KD}{1-D}. \tag{5}$$

Similarly, the average dc link voltage during one switching period is described by (6), which is equal to the C_2 voltage.

$$\bar{v}_{dc} = D(K v_{C_1} + v_{C_2}) = G v_{C_1} = v_{C_2}. \tag{6}$$

The maximum switch voltage stress at the primary side and secondary side are expressed by (7) and (8) respectively.

$$V^{\text{Primary}} = \frac{v_{in}}{1-D} \tag{7}$$

$$V^{\text{Secondary}} = \frac{K v_{in}}{1-D}. \tag{8}$$

IV. Soft-Switching and Active Voltage Clamping Circuit Analysis

The detailed equivalent circuit of a BBI is shown in Fig. 6, where L_σ is the total leakage inductance of the transformer and the capacitors C_{S1}, C_{Sp}, C_{Sq} and C^*_{INV} are the IGBT's output capacitors.

A. DC–AC Mode

In the DC-AC mode, the power is transferred from a fuel cell to the AC load. The main operating waveforms are shown in Fig. 7 and the operating stages during half a triangle carrier period are shown in Fig. 8.

First stage ($t_0 - t_1$): S_1 is OFF and the three-phase inverter operates in the shooting-through zero state. The positive magnetizing current i_{Lm} freewheels through the inverter's anti-parallel diodes. v_{cp} and v_{cq} are kept constant. Their values are $KV_{in} + \Delta V_{C_{p1}}$ and $V_{c2}/K + \Delta V_{C_{q1}}$ respectively.

Second stage ($t_1 - t_2$): S_1 is still OFF and the three-phase inverter is switched to the inverting state (S_{abcp}=110, S_{abcn}=001). The IGBTs S_{an}, S_{bn} and S_{cp} are turned off with ZCS because the magnetizing inductance current still freewheels through the anti-parallel diodes.

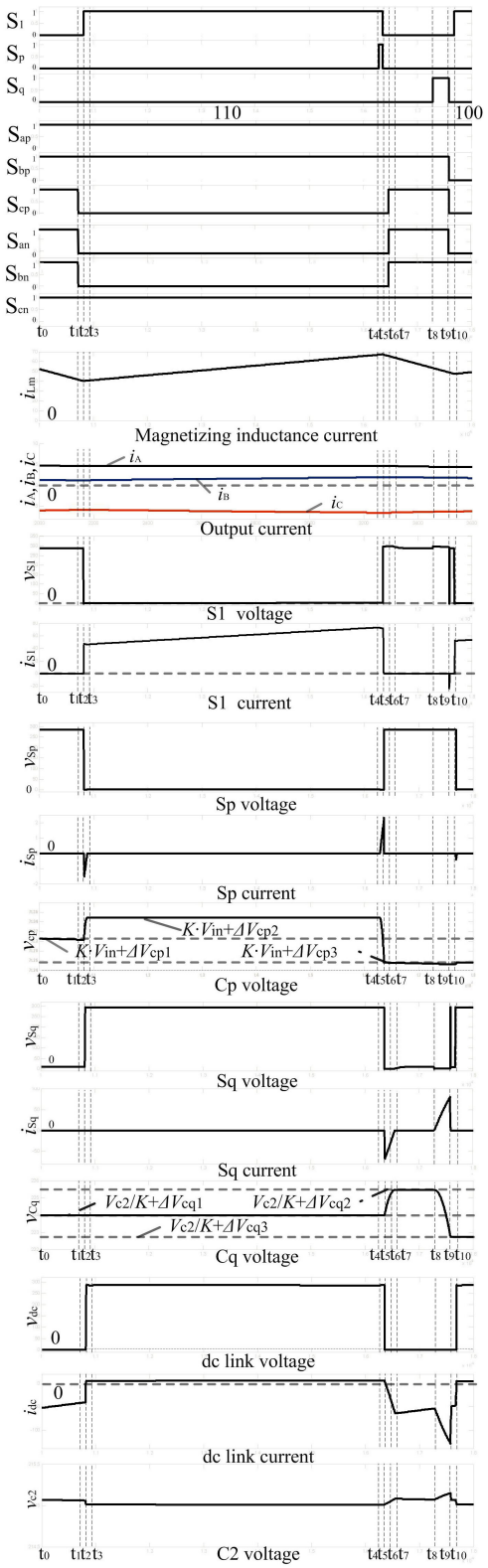

Fig. 7. DC–AC operating waveforms.

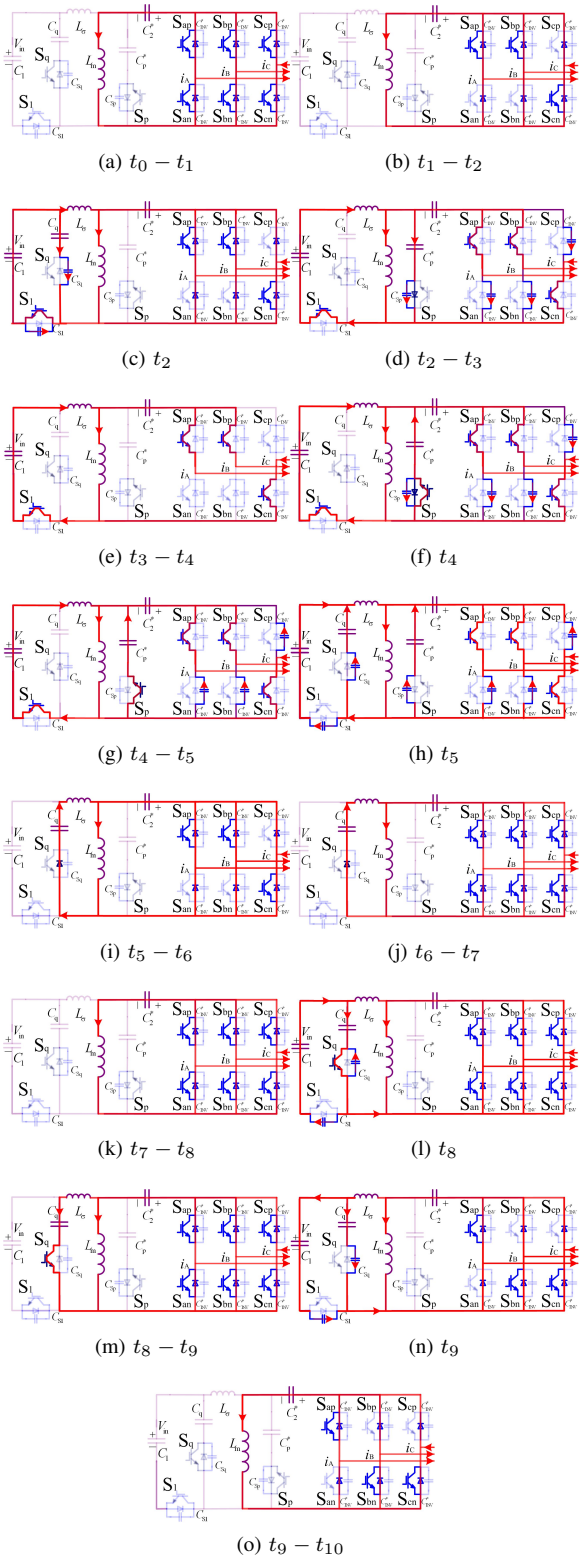

Fig. 8. DC-AC operating stages.

Third stage ($t_2 - t_3$): S_1 is turned on at t_2 as shown in Fig. 8 (c). C_{S1} is fast discharged from $V_{in} + V_{C_2}/K$ to zero and C_{sq} is fast charged from $\Delta V_{C_{q1}}$ to $V_{in} + V_{C2}/K + \Delta V_{C_{q1}}$. Because di/dt is weakened by the leakage inductance L_σ, the leakage inductance current i_{L_σ} begins to increase slowly. When the current i_{L_σ} is lower than $i_{Lm} + K\ (i_A + i_B)$, the three-phase inverter still keeps the shooting-through zero state. Although the shooting-through zero state changes in this stage, it is only illustrated that the anti-parallel diodes of the three-phase inverter are conducting. When the current i_{L_σ} exceeds $i_{Lm} + K\ (i_A + i_B)$ as shown in Fig. 8 (d), the output capacitors

S_{an}, S_{bn} and S_{cp} begin to be charged from zero to $KV_{in}+V_{c2}+\Delta V_{C_{p1}}$ and C_{sp} is discharged to zero. Then, the capacitor C_p continues to be charged to $KV_{in}+\Delta V_{C_{p2}}$ until the current i_{sp} drops to zero. C_p is so sufficient that the ripple voltage $\Delta V_{C_{p2}}$ is very small when compared to KV_{in}. The output capacitors S_{an}, S_{bn} and S_{cp} are also charged to $KV_{in}+V_{C2}+\Delta V_{C_{p2}}$. After that, C_{sp} is recharged to $\Delta V_{C_{p2}}$ and the inverter dc link voltage drops to $KV_{in}+V_{C2}$. Therefore, the active voltage clamping circuit for the three-phase inverter reduces the dc link spike voltage.

Fourth stage (t_3-t_4): During this period, the current i_{Lm} increases continuously.

Fifth stage (t_4-t_5): S_p is turned on at t_4 as shown in Fig. 8 (f). C_{sp} is fast discharged from $\Delta V_{C_{p2}}$ to zero and the output capacitors S_{an}, S_{bn} and S_{cp} are also charged to $KV_{in}+V_{C2}+\Delta V_{C_{p2}}$. Then, C_p is discharged from $K\cdot V_{in}+\Delta V_{C_{p2}}$ to $K\cdot V_{in}+\Delta V_{C_{p3}}$ and the output capacitors S_{an}, S_{bn} and S_{cp} are also discharged to $KV_{in}+V_{C2}+\Delta V_{C_{p3}}$. During this period, the leakage inductance current i_{L_σ} decreases.

Sixth stage (t_5-t_6): This stage starts when S_1 and S_p are turned off simultaneously, as shown in Fig. 8 (h). C_{s1} and C_{sq} begin to be charged and discharged respectively. The rate of voltage change depends on i_{L_σ} at t_5. C_{sp} and the output capacitors S_{an}, S_{bn} and S_{cp} also begin to be charged and discharged respectively. In addition, the rate of change is determined primarily by i_{Sp}. After the charging/discharging, as shown in Fig. 8 (i), the current i_{L_σ} is commutated to the anti-parallel diode of S_p and the current i_{Lm} is commutated to the anti-parallel diodes of the three-phase inverter. Moreover, C_q is charged from $V_{C2}/K+\Delta V_{C_{q1}}$.

Seventh stage (t_6-t_7): S_{an}, S_{bn} and S_{cp} are simultaneously turned on at t_6. The zero voltage turn-on is achieved by the gating on these devices while the anti-parallel diodes are conducting. C_q is charged to $V_{C2}/K+\Delta V_{C_{q2}}$ until i_{L_σ} drops to zero and C_{s1} is also charged to $V_{in}+V_{C2}/K+\Delta V_{C_{q2}}$. Finally, C_{sq} is recharged to $\Delta V_{C_{q2}}$, and C_{S1} is discharged to $V_{in}+V_{C2}/K$. According to the above analysis, the spike voltage of S_1 is restricted due to the active voltage clamping circuit.

Eighth stage (t_7-t_8): The three-phase inverter is still operating in the shooting-through zero state. The magnetizing current i_{Lm} keeps on decreasing at the rate of $V_{C2}/(K^2L_m)$, and C_2 is charged with a small voltage ripple.

Ninth stage (t_8-t_9): S_q is turned on at t_8, as shown in Fig. 8 (l). C_{Sq} is fast discharged from a low voltage $\Delta V_{C_{q2}}$ to zero and C_{s1} is charged to $V_{in}+V_{C2}/K+\Delta V_{C_{q2}}$. Then, C_q begins to resonate with L_σ, and C_q is discharged from $V_{C2}/K+\Delta V_{C_{q2}}$ to $V_{C2}/K+\Delta V_{C_{q3}}$.

Tenth stage (t_9-t_{10}): S_q, S_{an}, S_{bp} and S_{cp} are turned off at t_9. The zero current turn-offs are achieved by gating off S_{an} and S_{bp} while the anti-parallel diodes are conducting. After t_9, the current i_{L_σ} is commutated to the anti-parallel diode of S_1, and it decreases quickly until it drops to zero. Finally, C_{sq} is recharged to $\Delta V_{C_{q3}}$, and C_{S1} is discharged to $V_{in}+V_{C2}/K$.

B. AC–DC Mode

When the battery is charged, the power flows from the AC port to the DC side. Fig. 9 shows the main operating waveforms during one triangle carrier period. In this mode, the switches S_p and S_q still keep ZVS operation, but the magnetizing inductance current is reversed. Because the anti-parallel diode of S_1 is always conducting during the S_1 switching process, S_1 achieves ZCS and ZVS. A description

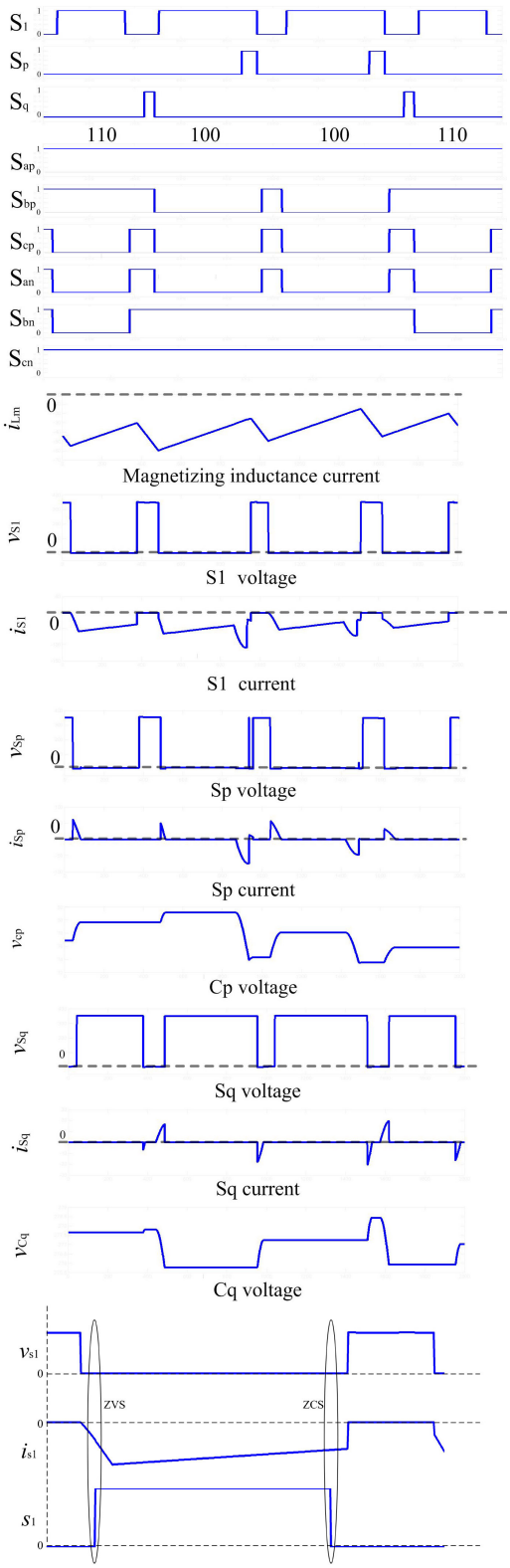

Fig. 9. AC–DC operating waveforms.

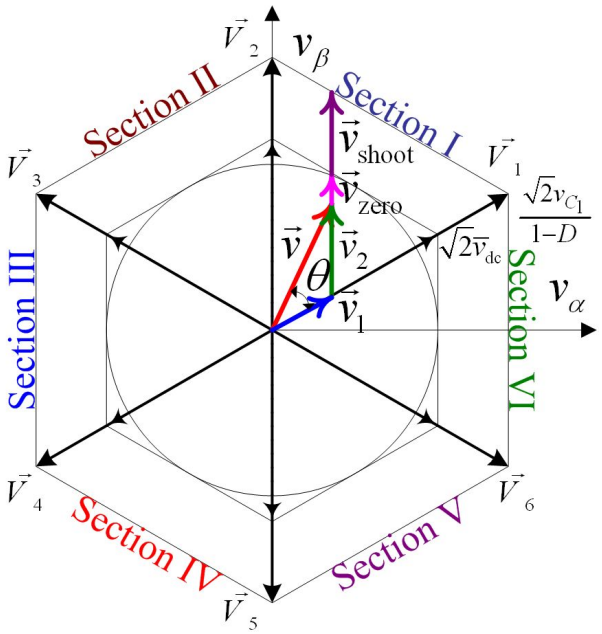

Fig. 10. Vectorial combination.

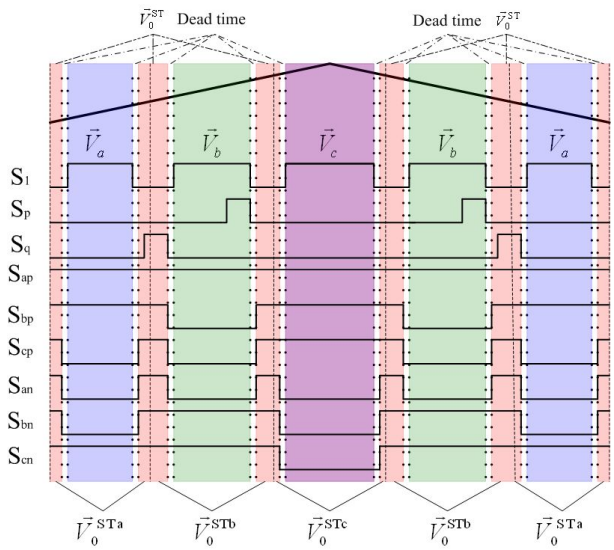

Fig. 11. Synchronous switching SVPWM.

of each stage can be analogously inferred and will not be discussed here.

V. The Modulation of a BBI

The line-to-line voltage space vectors of a BBI in the $\alpha-\beta$ coordinate system, listed in Table 1, are transformed from the line-to-line voltages v_{ab}, v_{bc} and v_{ca}. ρ represents the vector modulus and θ is the corresponding rotating angle. Although 21 effectual shooting-through zero vectors exist in a buck-boost inverter, the vector V_0^{ST} ($S_{abcp} = S_{abcn}$=111) is only used in the modulation. The vectorial combination of the line-to-line voltage vector $\vec{v}$ from section I, illustrated in Fig. 10, is described by the following formula:

$$\vec{v} = d_1\vec{V}_1 + d_2\vec{V}_2 + d_3\vec{V}_0 + d_4\vec{V}_0^{\mathrm{ST}} \tag{9}$$

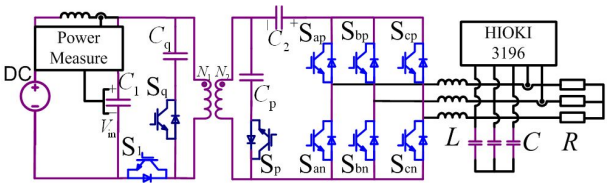

Fig. 12. Experimental schematic.

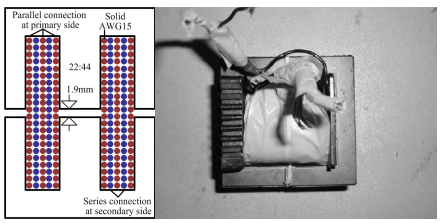

(a) Construction (b) Prototype

Fig. 13. BBI transformer in Forward-Flyback mode.

where, $\vec{V}_1$, $\vec{V}_2$ and $\vec{V}_0$ are the inverting state vectors, and $\vec{V}_0^{\mathrm{ST}}$ is the vector of the shooting-through zero state.

The corresponding vector duty cycles are written as

$$\begin{aligned} d_1 &= \sqrt{\frac{2}{3}}\frac{\rho\sin(\frac{\pi}{3}-\theta)}{v_{dc}} \\ d_2 &= \sqrt{\frac{2}{3}}\frac{\rho\sin\theta}{v_{dc}} \\ d_4 &= 1-D \end{aligned} \tag{10}$$

where, $d_1+d_2+d_3+d_4=1$, and $\rho \le \sqrt{3/2}Dv_{dc}$.

At the steady state, the phase peak voltage of the inverter is expressed as

$$v_{\mathrm{phase}}^{\mathrm{peak}} = \frac{MD}{2}v_{dc} = \frac{MG}{2}v_{C_1} \tag{11}$$

where, M is the modulation index, $M \in [0, 2/\sqrt{3}]$.

The buck boost factor of a BBI in buck-boost mode is expressed as:

$$BBF = \frac{MG}{2}. \tag{12}$$

TABLE I
Line-to-Line Voltage Space Vectors

S_1	S_A, S_B, S_C	v_{ab}, v_{bc}, v_{ca}	Vector	ρ	θ
1	10, 01, 01	$v_{dc}, 0, -v_{dc}$	V_1	$2^{0.5}v_{dc}$	30°
	10, 10, 01	$0, v_{dc}, -v_{dc}$	V_2		90°
	01, 10, 01	$-v_{dc}, v_{dc}, 0$	V_3		150°
	01, 10, 10	$-v_{dc}, 0, v_{dc}$	V_4	c	210°
	01, 01, 10	$0, -v_{dc}, v_{dc}$	V_5		270°
	10, 01, 10	$v_{dc}, -v_{dc}, 0$	V_6		330°
0	10, 10, 10	0, 0, 0	V_0	0	0°
	01, 01, 01	0, 0, 0			
	11, 11, 11	0	V_0^{ST}	0	

From (12), both the modulation index M and the buck-boost voltage gains G determine the buck-boost factor. When the fuel cell's output voltage drops with the load current, the BBI

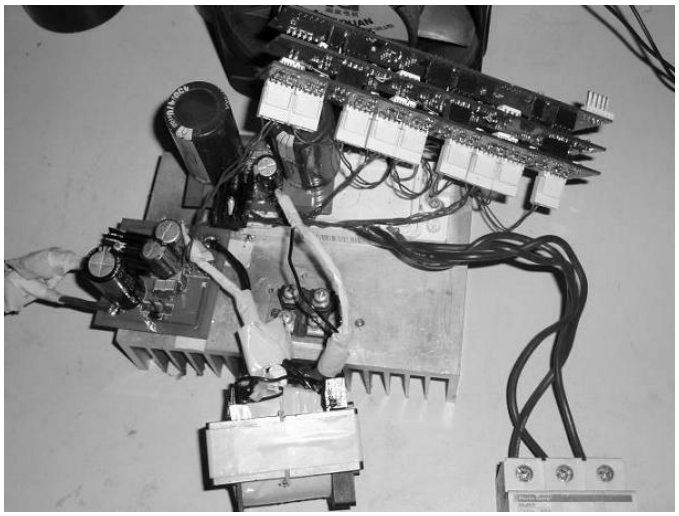

Fig. 14. BBI Prototype.

operating in buck-boost mode regulates the duty cycle of S_1 to control the dc link voltage of a conventional three-phase inverter, and the modulation index M is regulated to maintain the AC output.

Fig. 11 shows the switching sequence of synchronous switching SVPWM based on the triangular carrier method. This pulse width modulation is different from conventional SVPWM because the three-phase inverter's switches achieve ZVS and ZCS. During every switching period, there are five conventional vectors and six vectors of the shooting-through zero state in the symmetrical modulation. To avoid a short circuit between S_1 and the three-phase inverter, ten dead times should be inserted.

In this scheme, V_b is half of the maximum vector among $|V_1|$, $|V_2|$ and $|V_3|$, while V_c is the minimum vector. To reduce the inductance current ripple, the vectors of the shooting-through zero state distribute between the neighboring vectors, which is expressed as:

$$\frac{V_0^{STa}}{2V_a} = \frac{V_0^{STb}}{2V_b} = \frac{V_0^{STc}}{2V_c}. \tag{13}$$

To reduce the switching frequency, S_p can be merely turned on while the inverter operates at the V_b vector, and S_q can be turned on during the shooting-through zero state between the V_a and V_b vectors.

VI. Mathematical Analysis of BBI Circuit

When S_1 is turned off, the magnetizing current i_{Lm} charges the capacitor C_2 as shown in Fig. 8. The voltage ripple $\Delta V_{C2} \leq 0.01 V_{C2}$, is given by:

$$\Delta V_{C2} \leq \frac{\sqrt{3}}{4} \frac{DP_{in}}{V_{C2} f_C C_2} \tag{14}$$

where, P_{in} is the input power, D is the S_1 duty cycle, V_{C2} is the average voltage of C_2 and f_C is the triangle carrier frequency.

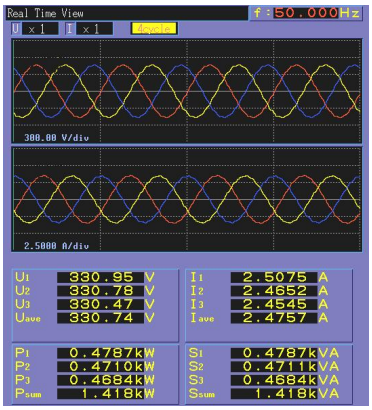

(a) load waveforms
(voltage: 300V/div, current: 2.5A/div)

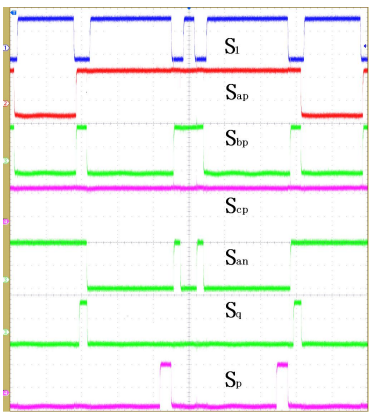

(b) IGBT drivers
(Voltage: 10V/div, time: 20μs/div)

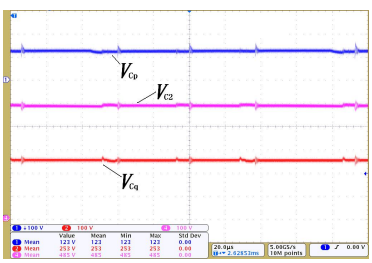

(c) Capacitors voltage
(Voltage: 100V/div; time: 20μs/div)

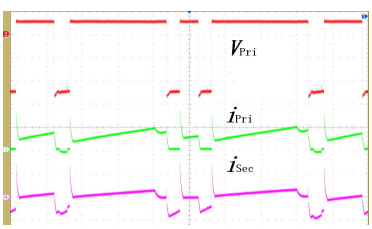

(d) Transformer waveforms
(Primary voltage $V_{\rm Pri}$, 100V/div; primary current $i_{\rm Pri}$, 50A/div; secondary current $i_{\rm Sec}$, 20A/div; time: 20μs/div)

Fig. 15. Experimental results.

During the C_q charging time $\tau_{\rm rise}(t_5 - t_7)$, the increased voltage $\Delta V_{C_{q2}}$ is calculated by

$$\Delta V_{C_{q2}} = \sqrt{\Delta V_{C_{q1}}^2 + \frac{L_{L_\sigma} i_{L_\sigma}^2}{C_q}}. \tag{15}$$

The rising time $\tau_{\rm rise}$ of the $\Delta V_{C_{q2}}$ is given by

$$\tau_{\rm rise} = \sqrt{L_\sigma C_q}\arctan\left(\sqrt{\frac{L_\sigma}{C_q}}\frac{i_{L_\sigma}}{\Delta V_{C_{q1}}}\right). \quad (16)$$

During the C_q discharging time $\tau_{Sq}(t8-t9)$, the decreased voltage $\Delta V_{C_{q3}}$ can be expressed by

$$\Delta V_{C_{q3}} = \Delta V_{C_{q2}}\cos\left(\frac{\tau_{S_q}}{\sqrt{L_{L_\sigma}C_q}}\right). \quad (17)$$

In addition, the reversed maximum current $i_{L_\sigma}^{\rm rev}$ can be calculated by

$$i_{L_\sigma}^{\rm rev} = \sqrt{\frac{C_q}{L_\sigma}}\Delta V_{C_{q2}}\sin\left(\frac{\tau_{S_q}}{\sqrt{L_{L_\sigma}C_q}}\right). \quad (18)$$

In order to minimize the increased voltage ΔV_{C_q}, the $\Delta V_{C_{q3}}$ must be zero. Therefore the switching-on time τ_{S_q} must be satisfied by:

$$\tau_{S_q} = \frac{\pi}{2}\sqrt{L_{L_\sigma}C_q}. \quad (19)$$

Combining (18) and (19), the reversed current is derived from:

$$i_{L_\sigma}^{\rm rev} = \sqrt{\frac{C_q}{L_\sigma}}\Delta V_{C_{q2}}. \quad (20)$$

The operation analysis of the clamping capacitor C_p is the same as that of the clamping capacitor C_q.

According to equations (15) and (20) and the modulation, three consecutive charges for C_p and C_q are implemented before they are discharged, and therefore the clamping capacitors can be calculated by:

$$C_{p,q} \geq 3\frac{L_\sigma I_{\rm max}^2}{\Delta V_{C_{p,q}}^2} \quad (21)$$

$$I_{\rm max} = I_{L_m} + KI_{\rm Phase} \quad (22)$$

where, I_{Lm} is the maximum value of the magnetizing current and $I_{\rm Phase}$ is the peak value of the output current.

VII. Experimental Results

A 1.5kW BBI prototype has been built to validate the proposed inverter, and the experimental schematic is shown in Fig 12. The main specifications and components are listed in Table 2, and the components' parameters are calculated according to (15)-(22). A DC source is used to simulate the fuel cell output characteristics, and the output voltage is regulated from 60V to 110V.

Fig. 13 (a) shows the construction of a transformer in forward and fly-back mode, where there are five layers of the same winding with 22 turns AWG15 solid copper wires to form the sandwich. The 3 parallel primary windings overlap with the 2 series-wound secondary windings to reduce the leakage inductance. The transformer prototype and the BBI prototype are shown in Fig. 13 (b) and Fig. 14 respectively.

Fig. 15 shows the experimental results, where the input voltage is 60V, the load resistor is 80Ω, M is 1.12 and D is 0.8. The load waveforms measured by a power quality analyzer HIOKI 3196 are shown in Fig. 15 (a). Fig. 15 (a) shows

TABLE II
1.5kW BBI Prototype Specifications

S_1	2 X IGBT IKW75N60T 600V/75A	C_p	$11.5\mu F/450$V
S_q	IGBT IKW75N60T	C_q	21μF/450V
Inverter	FP25R12KE3 1200V/25A	C_2	235μF/900V
S_p	GT15Q301 1200V/15A	ΔV_{Cp}	$\leq$16.5V
C_1	470μF/200V	ΔV_{Cq}	$\leq$12V
L	1mH ferrite		
C	40μF/450VAC CBB65B	ΔV_{C2}	$\leq$1V 530V
τ_{Sq}	4.4μs	τ_{Sp}	6.7μs
$f_{\rm Carrier}$	5kHz	f_{S1}	25kHz
Transformer	EE65 ferrite core, $N_1 : N_2 = 22 : 44$, total air gap 3.8mm, $L_m = 127\mu$H, $I_{Lm} = 55$A $L_\sigma = 0.4\mu$H (Primary side)		

the synchronous switching SVPWM in one switching cycle generated by the FPGA. Fig. 15 (c) shows that the C_2 voltage is boosted to 485V, while the output line-to-line voltage is 330.7V. The voltages of the clamping capacitors C_p and C_q are 123V and 253V respectively. These values are consistent with the theoretical values. The transformer waveforms during one switching period as shown in Fig. 15 (d) indicate that the transformer operates at the forward and fly-back mode.

The measured waveforms of the switch S_1 are shown in Fig. 16 (a), and the spike voltage of S_1 is clamped by S_p. Zero voltage turn-on of S_1 is shown in Fig. 16 (b) and the charge of C_{s1} during S_1 turn-off is shown in Fig. 16 (c). Fig. 16 (d)-(f) show the measured waveforms of the switch S_{an}, and that the spike voltage of S_{an} is clamped by S_q. Zero voltage turn-on and Zero current turn-off are shown in Fig. 16 (e) and (f) respectively. Fig. 16 (g) and (h) show the measured waveforms of the clamping switches S_p and S_q. Before S_p and S_q are turned on, the voltage of these switches have dropped to zero. Therefore, ZVS is achieved by gating on S_p and S_q. While the resonant current of the clamping circuit is reversed through the anti-parallel diode of the clamping switches, the ZCS is also achieved by gating off S_p and S_q.

The efficiency of the BBI system has been experimentally evaluated, and the system losses include the losses from the output filters (L and C) and the auxiliary circuits. The auxiliary circuits consist of transducers, gate drivers and a digital control board, and the total power consumed by auxiliary circuit is less than 10W. While the input voltage increases from 60V to 110V and the voltage gain is 5, the efficiency of the BBI increases from 85.84% to 87.54%, and output power increases from 550W to 1767W, as shown in Fig. 17 (a). When the voltage gain increases from 4 to 8 with 60V of input voltage, the efficiency changes from 84.5% to 86.2%, as shown in Fig. 17 (b). Therefore, the BBI performs with improved efficiency with a wide range of input voltages. Although the efficiency

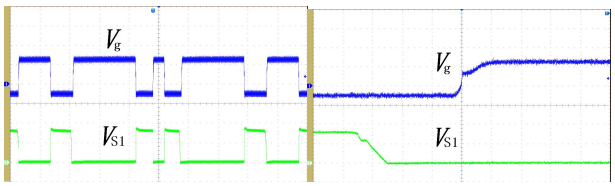

(a) S_1 clamping voltage

(b) S_1 zero voltage turn-on

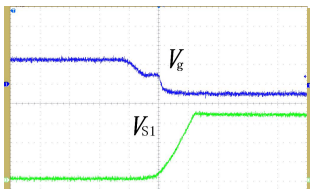

(c) C_{S1} charge during turn-off

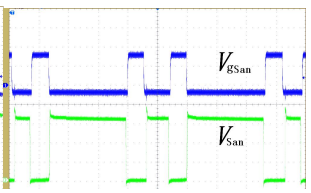

(d) S_{an} clamping voltage

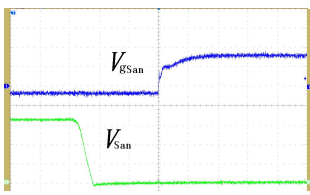

(e) S_{an} Zero voltage turn-on

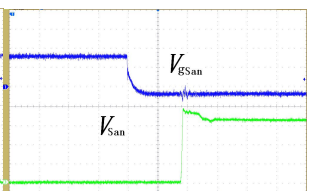

(f) S_{an} Zero current turn-off

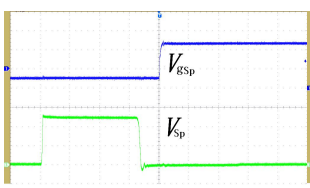

(g) Zero-voltage turn-on of S_p

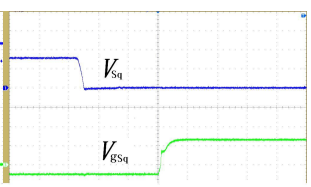

(h) Zero-voltage turn-on of S_q

Fig. 16. Soft-switching waveforms of the switches. V_{S1}, V_{San}, V_{sp}, V_{sq} (100V/div), V_g (10V/div)

of the prototype is not very high due to an unimproved transformer, it is worth expecting that the BBI's efficiency can be improved up to 92% by using an optimized transformer and circuit layout.

VIII. Conclusions

A new isolated soft-switching bidirectional buck-boost inverter has been proposed for fuel cell applications. The operation, analysis, features and design considerations have been presented. The experimental results for a 1.5kW, 25 kHz prototype verify the operation principle.

The main switches achieve ZVS and ZCS by using a novel synchronous switching SVPWM. The active clamping circuits reduce the spike voltages of the switches. The experimental results indicate that the inverter maintains efficient conversion with a wide range of input voltages and voltage gains. Therefore, the BBI is suitable for power applications that require a wide range of input voltages and voltage gains.

Acknowledgment

This work was supported by a key project for the National Supporting Technology: Power Electronic Devices and Power Integration (2007BAA12B01).

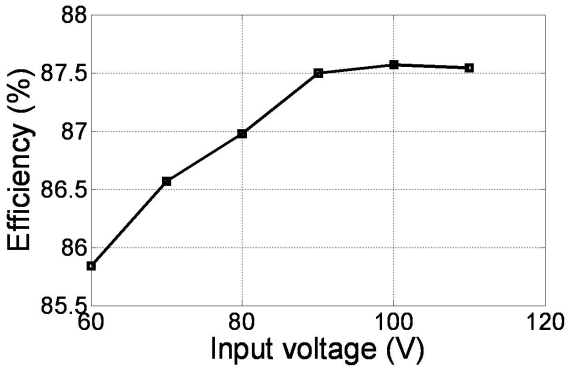

(a) Various input voltage

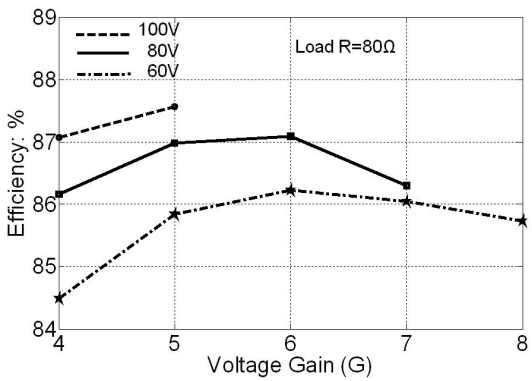

(b) various voltage gain G

Fig. 17. Efficiency of BBI.

References

[1] *DOE Fuel Cell Handbook*, 7^{th} ed., EG&G Technical Services Inc., Morgantown , WV, pp: 8.27-8.44, 2004.

[2] X. Yu, M. R. Starke, L. M. Tolbert, and B. Ozpineci, "Fuel cell power conditioning for electric power applications: a summary," *IETElectr. Power Appl.*, Vol.1, No. 5, pp. 643-656, Sep. 2007.

[3] S. K. Mazumder, R. K. Burra, and K. Acharya, "A ripple-mitigating and energy-efficient fuel cell power-conditioning system," *IEEE Trans. Power Electron.*, Vol. 22, No. 4, pp.1437-1452, Jul. 2007.

[4] P. T. Krein, R. S. Balog, and G. Xin, "High-frequency link inverter for fuel cells based on multiple-carrier PWM," *IEEE Trans. Power Electron.,* Vol. 19, No. 5, pp. 1279-1288, Sep. 2004.

[5] M. Marchesoni, C. Vacca, "New DC-DC converter for energy storage system interfacing in fuel cell hybrid electric vehicles," *IEEE Trans. Power Electron.,* Vol. 22, No. 1, pp. 301-308, Jan. 2007.

[6] R. J. Wai, R. Y. Duan, J. D. Lee, and L. W. Liu, "High-efficiency fuel-cell power inverter with soft-switching resonant technique," *IEEE Trans. Energy Convers.*, Vol. 20, No. 2, pp. 485-492, Jun. 2005.

[7] G. K. Andersen, C. Klumpner, S. B. Kjær, F. Blaabjerg, "A new power converter for fuel cells with high system efficiency," *International Journal of Electronics*, Vol. 90, No. 11, pp. 737-750, Nov. 2003.

[8] R. Gopinath, S.S. Kim, J. H. Hahn, P. N. Enjeti, M. B. Yeary, and J. W. Howze, "Development of a low cost fuel cell inverter system with DSP control," *IEEE Trans. Power Electron.*, Vol. 19, No. 5, pp. 1256-1262, Sep. 2004.

[9] S. Jang, C. Won, B. Lee, and J. Hur, "Fuel cell generation system with a new active clamping current-fed half-bridge converter," *IEEE Trans. Energy Convers.*, Vol. 22, No. 2, pp. 332-340, Jun. 2007.

[10] X. Kong, A. M. Khambadkone, "Analysis and implementation of a high efficiency, interleaved current-fed full bridge converter for fuel cell system," *IEEE Trans. Power Electron.*, Vol. 22, No. 2, pp. 543-550, Mar. 2007.

[11] S. Jung, Y. Bae, S. Choi, and H. Kim, "A low cost utility interactive inverter for residential fuel cell generation," *IEEE Trans. Power Electron.*, Vol. 22, No. 6, pp. 2293-2298, Nov. 2007.

[12] J. Wang, F. Z. Peng, J. Anderson, A. Joseph, and R. Buffenbarger, "Low cost fuel cell converter system for residential power generation," *IEEE Trans. Power Electron.*, Vol. 19, No. 5, pp. 1315-1322, Sep. 2004.
[13] J. L. Duarte, M. Hendrix, and M. G. Simões, "Three-port bidirectional converter for hybrid fuel cell systems," *IEEE Trans. Power Electron.*, Vol. 22, No. 2, pp. 480-487, Mar. 2007.
[14] J. Lee, J. Jo, S. Choi, and S. B. Han, "A 10-kW SOFC low-voltage battery hybrid power conditioning system for residential use," *IEEE Trans. Energy Convers.*, Vol. 21, No. 2, pp. 575-585, Jun. 2006.
[15] J. S. Lai, S. Y. Park, S. Moon, and C. L. Chen, "A high-efficiency 5-kW soft-switched power conditioning system for low-voltage solid oxide fuel cells," in *Proc. PCC '07 Conf.*, Nagoya Japan, pp. 463-470, 2007.
[16] H. M. Tao, J.L. Duarte, M.A.M. Hendrix, "Line-interactive UPS using a fuel cell as the primary source," *IEEE Trans. Ind. Electron.*, Vol. 55, No. 8, pp. 3012-3021, Aug. 2008.
[17] M.H. Todorovic, L. Palma, P.N. Enjeti, "Design of a wide input range DC–DC converter with a robust power control scheme suitable for fuel cell power conversion," *IEEE Trans. Ind. Electron.*, Vol. 55, No. 3, pp. 1247-1255, Mar. 2008.
[18] J. M. Kwon, B. H. Kwon, "High step-up active clamp converter with input-current doubler and output-voltage doubler for fuel cell power," *IEEE Trans. Power Electron.*, Vol. 24, No. 1, pp. 108-115, Jan. 2009.
[19] K.Jin, X.B. Ruan, "Hybrid full-bridge three-level LLC resonant converter – a novel DC-DC converter suitable for fuel-cell power system," *IEEE Trans. Ind. Electron.*, Vol. 53, No. 5, pp. 1492-1503, May 2008.
[20] J. Kikuchi and T. A.Lipo., "Three-phase PWM boost-buck rectifiers with power-regenerating capability," *IEEE Trans. Ind. Appl.*, Vol. 38, No. 5, pp. 1361-1369, Sep. 2002.
[21] C. T. Pan and J. J. Shieh, "A single-stage three-phase boost-buck AC/DC converter based on generlized zero-space vectors," *IEEE Trans. Power Electron.*, Vol. 14, No. 5, pp. 949-958, Sep. 1999.
[22] P.C.Loh., P.C.Tan., F.Blaabjerg., and T.K.Lee., "Topological development and operational analysis of buck-boost current source inverters for energy conversion applications," in *Proc. IEEE PESC'06 Conf.*, Soul Corea, pp. 1-6, 2006.
[23] C. Klumpner, "A new single-stage current source inverter for photovoltaic and fuel cell applications using reverse blocking IGBTs," in *Proc. IEEE PESC'07 Conf.* Orlando USA, pp. 1683-1689, 2007.
[24] F. Z. Peng, M. Shen, K. Holland, "Application of Z-source inverter for traction drive of fuel cell – battery hybrid electric vehicles," *IEEE Trans. Power Electron.*, Vol. 22, No. 3, pp. 1054-1061, May 2007.
[25] D. L. Chen. and L. Li, "Novel static inverters with high frequency pulse DC link," *IEEE Trans. Power Electron.*, Vol. 19, No. 4, pp. 971-978, Jul. 2004.
[26] K. Fukushima, T. Ninomiya, S. Abe, I. Norigoe, Y. Harada, K. Tsukakoshi, and Z. Dai, "Steady-state characteristics of a novel DC-AC converter for fuel cells," in *Proc. IEEE INTELEC'07 Conf.*, pp. 904-908, 2007.

Lianghua Zhang was born in Hubei Province, China in 1980. He received his B.S. and M.S. in Electrical Engineering from Xi'an Jiaotong University, China, in 2002 and 2005, respectively. Since 2005, he has been with the Department of Electrical Engineering, Xi'an Jiaotong University, where he is currently pursuing his Ph.D. in Engineering Science. His research interests are in the areas of power electronics integration, new circuit topologies, motion control systems, uninterruptible power supplies and dc-dc power supplies.

Xu Yang was born in China in 1972. He received his B.S. and Ph.D. in Electrical Engineering from Xi'an Jiaotong University, Xi'an, China, in 1994 and 1999, respectively. He has been a member of the faculty of the School of Electrical Engineering, Xi'an Jiaotong University since 1999, where he is presently a Professor. From November 2004 to November 2005, he was with the Center of Power Electronics Systems (CPES), Virginia Polytechnic Institute and State University, Blacksburg, VA, as a Visiting Scholar. He then came back to Xi'an Jiaotong University, and began teaching and doing research in the areas of power electronics and industrial automation. His current research interests include soft switching topologies, PWM control techniques, power electronic integration, and packaging technologies.

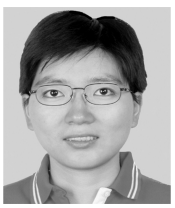

Wenjie Chen was born in Xi'an, China, in 1974. She received her B.S., M.S. and Ph.D. in Electrical Engineering from Xi'an Jiaotong University, Xi'an, China, in 1996, 2002 and 2006, respectively. She has been a member of the faculty of the School of Electrical Engineering, Xi'an Jiaotong University since 2002, where she is currently an Associate Professor. Her main research interests include soft-switching dc/dc converters and active filters, and power electronic integration.

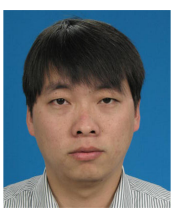

Xiaofeng Yao was born in Shaanxi, China, in 1985. He received his B.S. in Electronic Engineering from Xi'an Jiaotong University, China, in 2007, where he is currently pursuing his M.S. in the Power Electronics & Renewable Energy Research Center (PEREC). His main research interests include DC/DC converters and single-phase grid-connected inverters based on photovoltaic modules.